Atomistic simulation of thermomechanical properties of β-SiC

Meijie Tang and Sidney Yip
Department of Nuclear Engineering, Massachusetts Institute of Technology, Cambridge, Massachusetts 02139-4307
(Received 1 June 1995; revised manuscript received 11 August 1995)

A classical bond-order interatomic potential function developed by Tersoff has been applied to study the structural, mechanical, thermal, vibrational, and surface properties of β-SiC. The potential has been modified to eliminate the unphysical effects associated with large volumetric deformation. Fundamental bulk properties, e.g., phonon dispersion curves, thermal expansion coefficient, equation of state, elastic constants, as well as surface relaxation and reconstruction have been studied. Comparisons with available literature data indicate that the modified Tersoff potential gives a reasonably good description of the interatomic forces in β-SiC, including angle-dependent interactions, provided only nearest-neighbor interactions are allowed.

I. INTRODUCTION

In recent years, computer simulations have become an increasingly powerful tool for studying materials properties and behavior. While first-principles quantum mechanical methods generally give the most accurate results, they cannot be applied to problems such as melting at a grain boundary,[1] brittle-ductile transitions in crack tip extension,[2] and dislocation mobility[3] which require much larger system sizes or longer simulations. For these investigations, empirical many-body potentials can be used to provide useful first results, if only for scoping purposes.

Among covalent materials, Si has been studied most extensively because of its technological importance. A recent review[4] considering the six most frequently used empirical potentials of Si concluded that none of these potentials are totally accurate and transferrable. On the other hand, valuable insights into various physical properties can be gained using these potentials if proper interpretations are made which take into account the strength and weakness of each potential model. Thus the use of empirical potential models can give a first look at properties and behavior which are otherwise impossible to study by experiments or first-principles calculations.

SiC is another covalent material with atomic-level and electronic properties well suited for high power, high frequency, and high temperature applications. In recent years, the properties of SiC which have been studied in simulations include amorphous structure,[5,6] grain boundaries,[7] structure and mechanical behavior,[8,9] and radiation damage.[11] In contrast to elemental systems like Si and C, an additional interaction between Si and C needs to be taken into account. Three empirical potentials have been developed for SiC.[12–14] Tersoff developed a many-body bond-order type of potential for Si (Ref. 15) and C.[16] Later, the same formalism was adapted for SiC.[12] Pearson and co-workers developed a model consisting of two-body and three-body interactions[13] and Baskes developed a modified embedded-atom model (EAM) type of potential.[14] Some applications have been made already using these empirical potentials.[6,11,8,9] However, little can be said about the accuracy and transferability of these models. In particular, the applicability of using these potentials to study the mechanical behavior of β-SiC under large deformation has not been investigated.

In this paper, we present a study of bulk and surface properties of β-SiC using a modified form of the Tersoff potential. For surface relaxation and reconstruction, the results obtained using the Pearson potential are also given for comparison. We first describe the Tersoff potential and discuss its modification in Sec. II. The results for bulk and surface properties, namely, phonon dispersion curves, equation of state, thermal expansion coefficient, elastic constants, and surface relaxation and reconstruction are presented in Sec. III. Except for calculations at 0 K, all results are obtained by molecular dynamics simulations. For bulk properties, we use 216 atoms arranged in a cubic simulation cell with periodic boundary conditions. The time step we use is 1.45×10^{-4} ps. Typical calculations run for 30 000 steps except those for elastic constants calculations which run for about 100 000 to 300 000 steps. For constant pressure simulations, we use the method of Parrinello and Rahman.[17,18] Discussion and conclusion are given in Sec. IV.

II. TERSOFF POTENTIAL

A. Bond order

The Tersoff potential is based on the bond-order concept.[19] The interatomic potential energy between two neighboring atoms i and j is written as[12]

$$V_{ij}=f_c(r_{ij})[A\exp(-\lambda r_{ij})-\chi B b_{ij}\exp(-\mu r_{ij})] \quad (1)$$

where b_{ij} is the many-body bond-order parameter describing how the bond-formation energy (the attractive part of V_{ij}) is affected by local atomic arrangement due to the presence of other neighboring atoms—the k atoms. It is a many-body function of the positions of atoms i, j, and k. It has the form[12]

$$b_{ij}=(1+\zeta_{ij}^{n_i})^{-1/2n_i}, \quad (2)$$

$$\zeta_{ij}=\sum_{k\neq i,j} f_c(r_{ik})\beta_i g(\theta_{ijk}) \quad (3)$$

where ζ_{ij} is called the effective coordination number and $g(\theta_{ijk})$ is a function of the angle between $\vec{r}_{ij}$ and $\vec{r}_{ik}$ which

0163-1829/95/52(21)/15150(10)/$06.00 © 1995 The American Physical Society

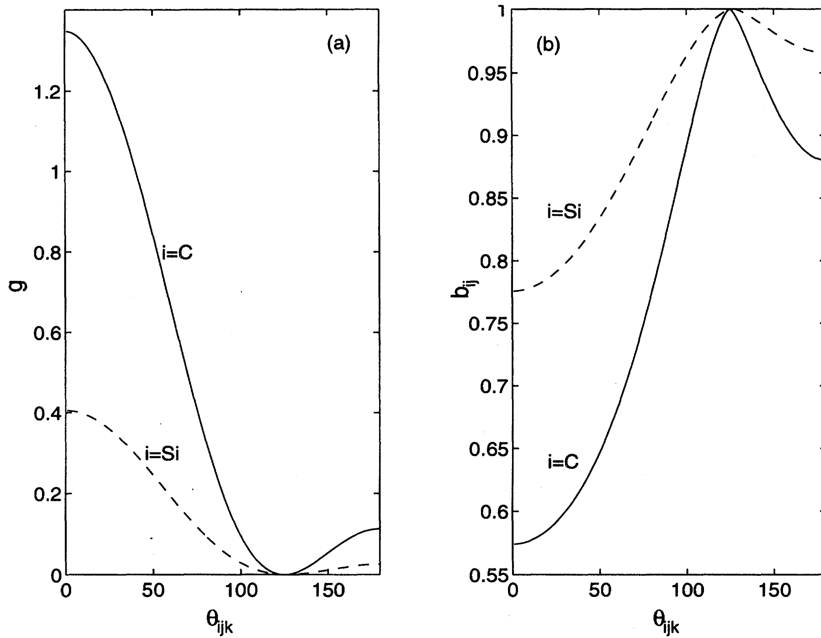

FIG. 1. (a) Angular function $g(\theta_{ijk})$ and (b) bond-order parameter b_{ij} in Tersoff potential.

has been fitted to stabilize the tetrahedral structure. The larger the b_{ij}, the stronger is the bond, and the more attractive is the interaction between atoms i and j. In this description the bond strength between atoms i and j is determined not only by the distance r_{ij} but also by the competition from interactions between atoms i and k through b_{ij}.

The binding between i and k atoms affects the binding strength of V_{ij} in three ways. First, the larger the distance r_{ik}, the smaller is the competition from atom k. This distance dependence is described by a quasi-step-function (the same as the cutoff function f_c) in the Tersoff potential. Secondly, the angle θ_{ijk} between $\vec{r}_{ik}$ and $\vec{r}_{ij}$ has a particular effect on strengthening the bond between i and j. If we take a three-atom triplet as an example, the angular function $g(\theta_{ijk})$ and the angular dependence of b_{ij} are shown in Fig. 1 for $r_{ij}=r_{ik}=1.87$ Å (1.87 Å is the equilibrium nearest-neighborbond length in β-SiC). The solid lines are obtained when the center atom i is C and the two j atoms are Si; the dashed lines are obtained when the center atom i is Si and the two j atoms are C. One sees that at small angles the angular functions are large and the corresponding bond-order parameter is small. This means that two adjacent bonds with a small enclosed angle are weakened more significantly by bond ordering than the bonds with large angles enclosed. Thirdly, given the same distance and angle, the more neighboring k atoms, the weaker is the binding between i and j. The coordination number dependence of b_{ij} is shown in Fig. 2 given all $r_{ij}=r_{ik}=1.87$ Å and all $\theta_{ijk}=109.47°$ (the tetrahedral angle).

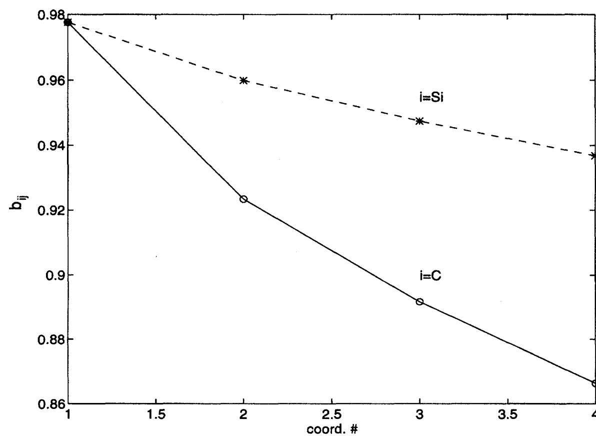

FIG. 2. Coordination number dependence of bond-order parameter b_{ij}.

Using the Tersoff potential, we first calculate the equilibrium properties of β-SiC at 0 K. The results are shown in Table I along with the results obtained from the Pearson potential, the modified EAM potential, a tight-binding model,[20] and experimental data. The methods of elastic constants calculation will be discussed later in Sec. III. The com-

TABLE I. Comparison of β-SiC properties obtained from the Tersoff potential (TP), Pearson potential (PP), modified EAM potential (MEAM), tight-binding method (TBA), and experiment (Expt.). r is the lattice parameter; E is the cohesive energy; and B is the bulk modulus.

	TP	PP	MEAM	TBA	Expt.
r (Å)	4.32	4.19	4.2	4.36	4.36[a]
E (eV)	−6.18	−7.71	−6.4		−6.34[a]
B (Mbar)	2.25	9.90	2.11	2.29	2.25[b]
C_{11} (Mbar)	4.36	10.95		3.72	3.90[b]
C_{12} (Mbar)	1.20	9.37		1.57	1.42[b]
C_{44} (Mbar)	2.55	6.06	2.05	2.56 (unrelaxed)	2.56[b]

[a]A. R. Verma and R. Krishna, *Polymorphism and Polytypism in Crystals* (Wiley, New York, 1966), pp. 103.
[b]Reference 35.

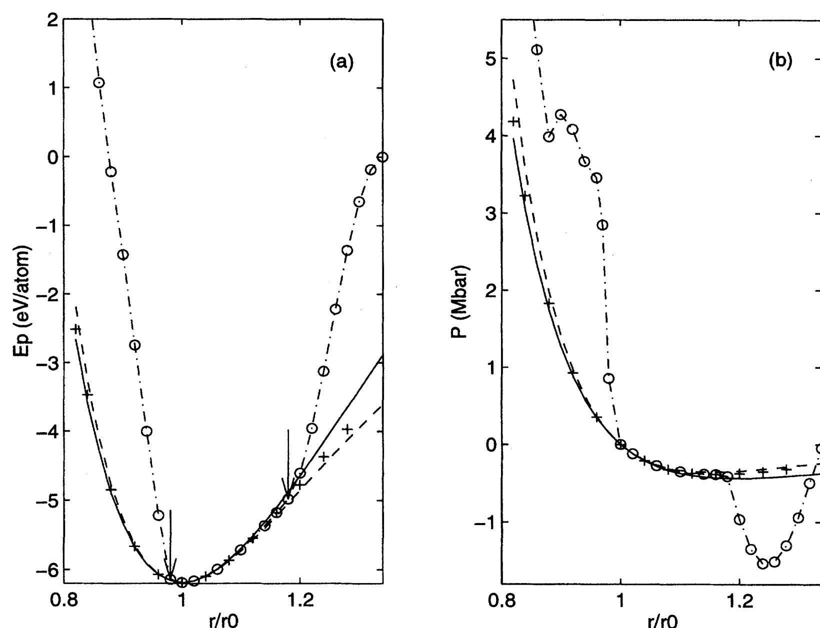

FIG. 3. Comparison of (a) cohesive energy (eV/atom) and (b) pressure of β-SiC under deformation at 0 K obtained by *ab initio* calculation (solid line), universal binding curve (dashed line), original Tersoff potential (circles, chained line is to guide the eyes), and modified Tersoff potential (crosses).

parisons show that the Tersoff potential describes the equilibrium properties such as cohesive energy and elastic constants of β-SiC quite well. (Note that, except for the cohesive energy, none of the properties are directly fitted in developing the potential.) Importantly, the Tersoff potential predicts accurately the shear elastic constant C_{44}, suggesting that the angular forces are satisfactorily described by the model.

B. Cutoff and modification

The Tersoff potential was developed using a fixed short-ranged cutoff which allows only the nearest neighbors to interact at zero pressure equilibrium condition. One obvious drawback of this cutoff is that it cannot describe the energy difference between β-SiC and its polytypisms such as α-SiC since they differ only in long-range stacking sequence. In addition, we have found unphysical effects due to the short-ranged cutoff at large volumetric deformation under pressure. The effects are clearly seen in Figs. 3(a) and 3(b), which compare the cohesive energy and pressure curves obtained from the Tersoff potential, the universal binding curve,[21] first-principles energy calculation,[22] and the modified Tersoff potential (to be discussed later). The arrows in Fig. 3(a) indicate the deformed states beyond which the Tersoff potential begins to deviate significantly from the first-principles calculation results and the universal binding curve. (Corresponding unphysical behavior also show up in the pressure curve.) In the region in between, the agreement with both first-principles calculation and the universal binding curve is good.

At the right arrow, the cutoff function f_c ceases to be unity and begins to take the cosine form (see Ref. 12 for the expression of f_c). This occurs at a state of $r/r_0 = 1.18$ which is beyond the critical value of $r/r_0 = 1.158$ predicted by elastic instability analysis.[9,10] This means that the unphysical effect on the right is irrelevant as far as volumetric deformation under tension is concerned.

At the left arrow, an abrupt kink appears at $r/r_0 = 0.984$ which is not far from the zero pressure equilibrium configuration. The abrupt jump in the cohesive energy at the left arrow is caused by the sudden inclusion of the second-nearest-neighbor Si-Si interactions. At small deformation, $r/r_0 > 0.984$, each atom interacts with four nearest neighbors. Under large deformation, second nearest neighbors between Si-Si begin to interact with each other. Thus each Si atom interacts with four C atoms and 12 Si atoms, while each C still interacts with four Si atoms (the C-C cutoff is smaller).

To see how the second-nearest-neighbor interactions between Si-Si cause the abrupt increase of cohesive energy, we show in Fig. 4 the variation of the effective coordination number ζ_{ij}, the bond-order parameter b_{ij}, the interatomic binding energies V_{ij}, and the atomic potential energies U_i. The atomic potential energies are defined as $U_{\mathrm{Si}} = \Sigma_j V_{\mathrm{Si}\text{-}j}$ and $U_{\mathrm{C}} = \Sigma_j V_{\mathrm{C}\text{-}j}$. The cohesive energy of the system can then be written as $E_{\mathrm{coh}} = (1/2)(U_{\mathrm{Si}} + U_{\mathrm{C}})$. Figure 4(a) demonstrates that the abrupt increase of the cohesive energy comes from U_{Si}, not from U_{C}. This is because for the entire range studied each C always interacts with four neighbors whereas the number of neighbors of Si changes from 4 to 12 at $r/r_0 = 0.984$. For U_{Si}, the contributions from both $V_{\mathrm{Si\text{-}Si}}$ and $V_{\mathrm{Si\text{-}C}}$ are shown in Fig. 4(b). When $r/r_0 > 0.984$, $V_{\mathrm{Si\text{-}Si}} = 0$ and $V_{\mathrm{Si\text{-}C}}$ varies smoothly with compression. Comparing Figs. 4(a) and 4(b), one clearly sees that the abrupt energy increase is due to the first-nearest-neighbor interaction $V_{\mathrm{Si\text{-}C}}$, instead of the second-nearest-neighbor interaction $V_{\mathrm{Si\text{-}Si}}$. The contribution from the latter is actually very small. However, though the interaction between Si-Si is relatively weak, it has a significant effect on the first-nearest-neighbor Si-C interaction. The sharp energy increase means a strong weakening of the Si-C bond due to the formation of the 12 Si-Si bonds. ("Bond" here is simply defined by the interatomic distance; if the separation is less than the cutoff, a bond is formed. The stronger the bond, the lower is the en-

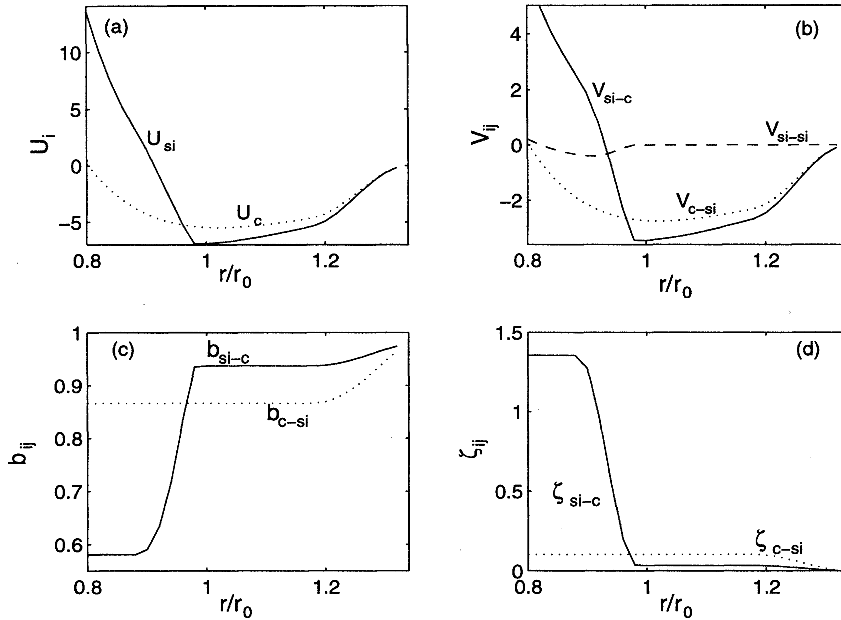

FIG. 4. Variations of (a) potential energies of Si and C; (b) effective pair energies of $V_{\text{Si-C}}$, $V_{\text{C-Si}}$, and $V_{\text{Si-Si}}$; (c) bond-order parameter b_{ij}; and (d) effective coordination number ζ_{ij}.

ergy.) As shown in Figs. 4(c) and 4(d), the weakening effect enters through the dramatic decrease of $b_{\text{Si-C}}$ due to an increase of $\zeta_{\text{Si-C}}$.

Further examination has shown that the extent to which the 12 Si-Si bonds weaken the Si-C bond depends on the angles they form with the Si-C bond. Among the 12 angles, three have a value of 35.26°, another three at 125.26°, and six at 90°. Because the angular functions shown in Fig. 1 favor small angles, the dominant contribution to the increase of $\zeta_{\text{Si-C}}$ comes from those Si-Si bonds with angles of 35.26°. Geometrically, the local interatomic configuration in the zinc-blende structure is a tetrahedron shown in Fig. 5, where the angles between the Si-C bond (thick solid line) and the three Si-Si bonds (thin solid line) are 35.26°. Therefore, under volumetric deformation with $r/r_0 < 0.984$, the additional interactions of the Si-Si bonds in the same tetrahedron cause significant weakening of the Si-C bond. The Si-C bond becomes much more repulsive when the Si-Si interactions are considered.

Si-Si interaction in the zinc-blende structure arises in a direct way when deformation under compression is considered. Since the Si-Si cutoff is held fixed, at a certain point during compression, Si-Si interaction will come into play and cause an abrupt change of the cohesive energy, pressure, and elastic constants. Another way that Si-Si can interact is at finite temperatures. Since the Si-Si cutoff (3.0 Å) is very close to the Si-Si distance (3.05 Å) under zero pressure at 0 K, thermal fluctuations can bring the atoms to within the interaction range. When one takes time averaged quantities as calculated properties, the effect of Si-Si interaction is included. This effect is most clearly seen in the strange behavior of elastic constants at finite temperatures, shown by the crosses in Fig. 10 below.

To eliminate the problem caused by the inclusion of the Si-Si interactions, one could in principle incorporate all three types of interactions, Si-C, Si-Si, and C-C, even at the zero pressure configuration and refit the Tersoff potential for β-SiC. Here, we propose a simple, intuitive modification involving using variable cutoffs. The idea is to restrict the interactions to only nearest neighbor as long as the system has the zinc-blende structure. This is reasonable for covalent materials since the binding is formed by sp^3 hybridized orbitals of nearest neighbors. We therefore scale the cutoffs with the system volume

$$R = R_0 \left(\frac{V}{V_0} \right)^{1/3} \tag{4}$$

where R_0 and V_0 are the cutoff and system volume at zero pressure at 0 K; R and V are the rescaled cutoff and system volume in a deformed state. The same rescaling rule applies to all the cutoff distances involved in the Tersoff potential. Interestingly, the cohesive energy and the pressure curves obtained using this modified Tersoff potential agree very well with the first-principles calculations and the universal binding curve, as shown in Fig. 3.

Our rescaling does not eliminate the problem of Si-Si interaction caused by thermal fluctuations because the Si-Si

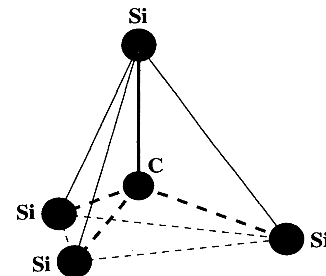

FIG. 5. Local atomic tetrahedron with a C atom at the center. The angles between the Si-C bond (thick solid line) and the three Si-Si bonds (thin solid line) are 35.26°.

TABLE II. Cutoff values (in units of Å) for β-SiC at zero pressure and at 0 K.

	$R_{\text{C-C}}$	$S_{\text{C-C}}$	$R_{\text{Si-Si}}$	$S_{\text{Si-Si}}$	$R_{\text{C-Si}}$	$S_{\text{C-Si}}$
Modified	1.93	2.13	2.60	2.80	2.36	2.56
Original	1.80	2.10	2.70	3.00	2.20	2.51

cutoff is too close to the Si-Si separation in the β-SiC structure. Furthermore, since the cutoffs in the Tersoff potential are not systematically fitted, by using the rescaling rule, one has some freedom to choose the cutoffs under zero pressure and at 0 K. We have chosen a set of cutoffs with the rescaling rule by fitting the melting temperature of our model to be around 5000 K, suggested by a Car-Parrinello molecular dynamics (MD) study.[5] The combination of Eq. (4) and the new cutoffs , listed in Table II, constitutes our modification of the Tersoff potential. In the following sections, we will present results of bulk and surface properties of β-SiC studied using this modified Tersoff potential.

III. RESULTS AND DISCUSSION

A. Phonon dispersion curves

Phonon dispersion curves of β-SiC at 0 K are obtained by evaluating the force constants $\partial U/\partial r_{i\alpha}\partial r_{j\beta}$, where U is the total potential energy of the system and $i,j=1,2,\ldots,N$, $\alpha,\beta=x,y,z$. The present results are compared with values obtained from a tight-binding calculation[23] as shown in Table III. Diagonalization of the dynamical matrix[24] yields the dispersion curves given in Fig. 6 along with the tight-binding result[23] and experimental data.[25] We see that the acoustic modes are very well described by the Tersoff potential. However, the optic modes are underestimated and the order of transverse and longitudinal modes is reversed for the Tersoff potential. Also, the optic modes at the Γ point are degenerate, in contrast to a pronounced splitting clearly seen in the experimental data and the tight-binding calculation, caused by the electric field induced by ionicity in SiC.[26] Since the Tersoff potential treats β-SiC as a fully covalent material, it is intrinsically unable to describe the splitting of the optic modes at Γ. Therefore the Tersoff potential gives a satisfactory description of the acoustic phonon dispersion curves, but the optic modes are not correctly described.

B. Equation of state

In this section, we present equation of state results for β-SiC under hydrostatic compression at room temperature (300 K). Corresponding results for hydrostatic tension have been published elsewhere.[8] Figure 7 shows the pressure-volume (P-V) curve compared with two sets of experimental data obtained by Bassett *et al.*[27] and Yoshida *et al.*,[28] respectively. The lines in the figure are fitted functions from the data using the Birch-Murnaghan equation of state[29]

$$P=\tfrac{3}{2}k_0[(V_0/V)^{7/3}-(V_0/V)^{5/3}]\times[1-\tfrac{3}{4}(4-k_0')\{(V_0/V)^{2/3}-1\}] \quad (5)$$

where V_0 and V are the volumes at zero pressure and under deformation, respectively, k_0 is the isothermal compressibility, and k' is the pressure derivative of k_0. Note that a simpler Murnaghan equation of state,

$$P=k_0/k_0'[(r_0/r)^{3k_0'}-1], \quad (6)$$

TABLE III. Elements of force constant matrix (in units of eV/Å^2) between nearest neighbors in β-SiC. $D_{\alpha\alpha}$ stands for D_{xx}, D_{yy}, and D_{zz}; $D_{\alpha\beta}$ stands for D_{xy}, D_{xz}, D_{yx}, D_{yz}, D_{zx}, and D_{zy}.

	Lee and Joannopoulos (Ref. 23)	Tersoff (Refs. 15,16)
$D_{\alpha\alpha}$	−5.66	−7.59
$D_{\alpha\beta}$	−3.08	−3.37

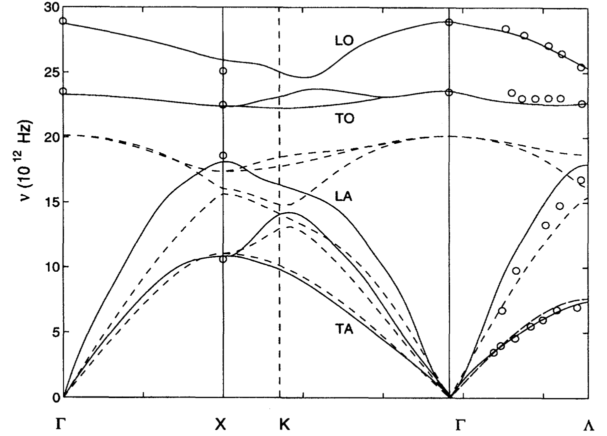

FIG. 6. Phonon dispersion curves of β-SiC at 0 K and under zero pressure obtained from tight-binding calculation (solid line), Tersoff potential (dashed line), and experimental data (circles).

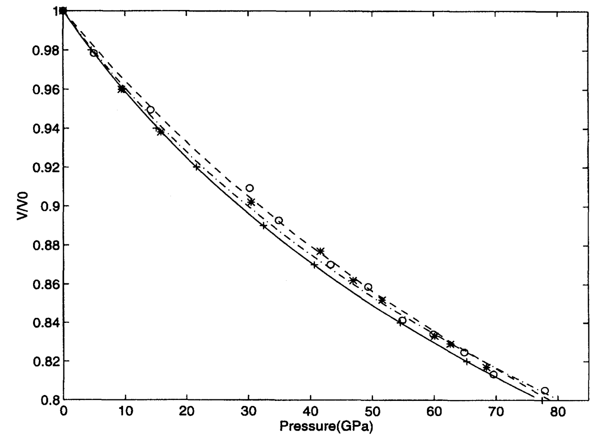

FIG. 7. Pressure-volume curves for β-SiC under compression. Circles and dashes line are data and fitted function obtained by Yoshida *et al.* (Ref. 28); stars and chained line are data and fitted function obtained by Bassett *et al.* (Ref. 27); crosses and solid line are data and fitted function from the modified Tersoff potential.

TABLE IV. Comparison of bulk modulus k_0 and its pressure derivative k_0' obtained by different studies.

	k_0(GPa)	k_0'
Present study	219±1	4.11±0.05
Yoshida *et al.* (Ref. 28)	260±9	2.9±0.3
Bassett *et al.* (Ref. 27)	230±4	4.0 (fixed)

is only valid in the low pressure region and it fails to properly describe the equation of state for the pressure region examined here. On the other hand, the Birch-Murnaghan equation of state provides a good description for both low and high pressure regions. As Fig. 7 shows, all the data can be fitted by the Birch-Murnaghan equation of state very well. Comparing the fitted parameters k_0 and k_0' from the three sets of data in Table IV, we find that there is good agreement between the modified Tersoff potential and the experimental data. This suggests that the modified Tersoff potential describes well the homogeneous response of β-SiC to hydrostatic compression.

C. Thermal expansion

So far, we have discussed properties of β-SiC at low temperatures, 0 K and 300 K. We now consider the temperature variation of the lattice constant of β-SiC up to 1500° K at zero pressure. A Parrinello-Rahman MD simulation[17] is performed at each temperature to determine the corresponding zero pressure lattice constant. The results, shown in Fig. 8, agree with experimental data[30] to within 1%. Both simulation and experiment[30] data can be fitted to polynomial functions of temperature, giving, respectively,

$$a(\text{nm}) = 0.432\,53 + 2.4719\times10^{-6}T + 1.5980\times10^{-10}T^2 + 1.0706\times10^{-14}T^3, \quad (7)$$

$$a(\text{nm}) = 0.435\,77 + 1.3887\times10^{-6}T + 7.8494\times10^{-10}T^2 - 2.4434\times10^{-13}T^3. \quad (8)$$

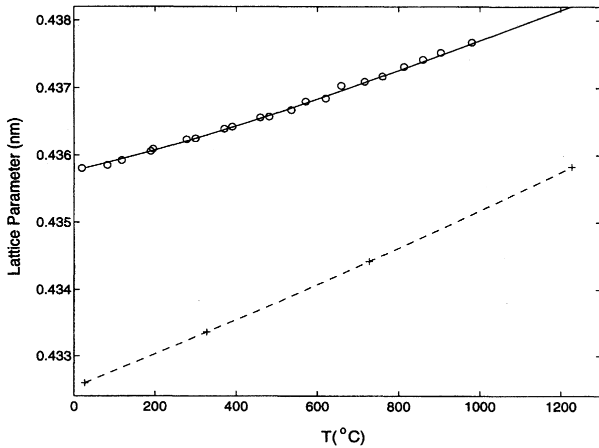

FIG. 8. β-SiC lattice constant versus temperature. Circles are experimental data; the solid line is fitted from circles; crosses are simulation data; and the dashed line is fitted from crosses.

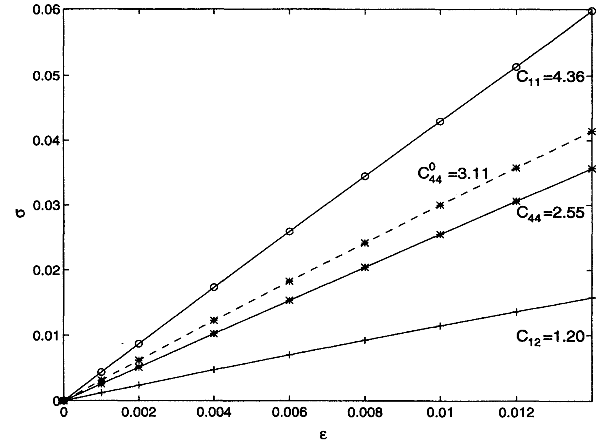

FIG. 9. Stress-strain curves for elastic constants calculations. Circles are data for C_{11}; crosses are for C_{12}; and stars are for C_{44} and C_{44}^0. C_{44}^0 is calculated without internal strain relaxation.

The linear temperature coefficient, $\partial a/\partial T$, determined from Eq. (7) and Eq. (8) are respectively 2.5×10^{-6} nm K^{-1} and 1.4×10^{-6} nm K^{-1}. This shows that the modified Tersoff potential produces a sufficiently good thermal expansion coefficient.

D. Elastic constants

The structural stability of a crystal when the system is under no external loading[31] is governed by elastic constants. The comparison of the calculated moduli provides a meaningful test of the interatomic potential function. We have determined the elastic constants at 0 K using straightforward stress-strain relations. For finite temperatures, we have derived fluctuation formulas[18] for the Tersoff potential. These results have not been reported previously to our knowledge. They have been used in the analysis of elastic instability for covalent materials.[8,9,32]

We have studied the elastic constants of β-SiC under zero pressure up to about 2000 K. The results of the stress-strain curves at 0 K are shown in Fig. 9. The elastic constants are determined from the slopes of these curves, e.g., $C_{11}=\sigma_{xx}/\epsilon_{xx}$, $C_{12}=\sigma_{xx}/\epsilon_{yy}$, $C_{44}=\sigma_{yz}/2\epsilon_{yz}$. Note that two values, C_{44} and C_{44}^0, are calculated for the shear elastic constant. C_{44}^0 is the shear elastic constant without internal strain relaxation,[33] whereas C_{44} is the shear elastic constant with full internal strain relaxation and therefore corresponds to the measured experimental value. In our calculation, internal strain relaxation is carried out by static relaxation, i.e., moving the Si and C atoms relative to each other until the forces on each atom vanish. The unrelaxed and relaxed values of C_{44} are 3.11 and 2.55 Mbar, respectively. For reasons of symmetry,[33] internal strain relaxation does not affect C_{11} and C_{12}. Using the fluctuation formulas, we have confirmed that at 0 K the Born term gives the same values for C_{11}, C_{12}, and the unrelaxed shear elastic constant C_{44}^0 as found from the stress-strain curves. We will show below that the effect of internal relaxation is described by the stress fluctuation term in the fluctuation formula.

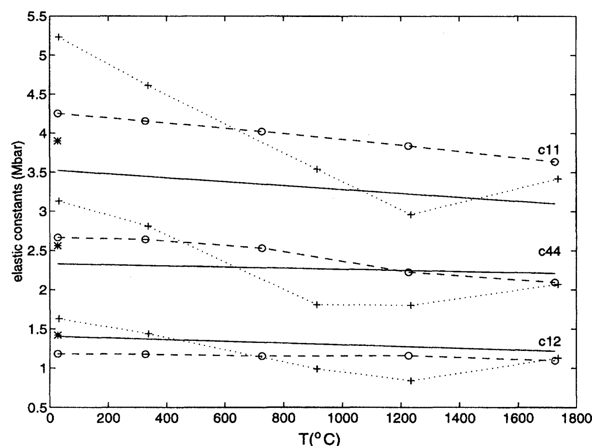

FIG. 10. Temperature variation of elastic constants of β-SiC obtained from the modified Tersoff potential (circles); results of Li and Bradt (Ref. 30) (solid line); and original Tersoff potential (crosses). The dashed line is fitted from the circles and the dotted line is to guide the eyes. Stars are experimental data of β-SiC at 300 K.

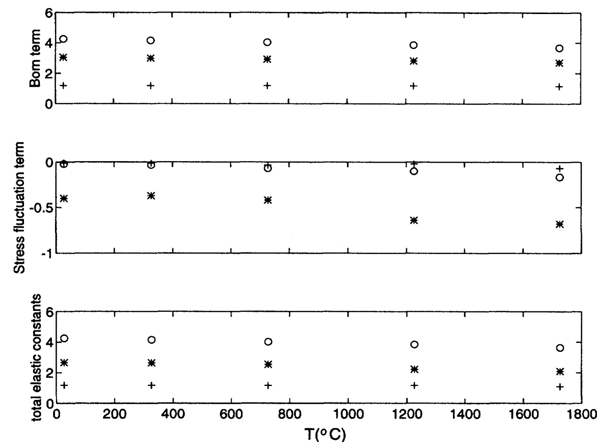

FIG. 11. The Born term, stress fluctuation term, and total elastic constants of β-SiC as a function of temperature. Circles are data for C_{11}; crosses are data for C_{12}; and stars are data for C_{44}. Notice the larger values of stress fluctuation term of C_{44} compared to that of C_{11} and C_{12}.

For elastic constant calculations at finite temperatures, we perform molecular dynamics simulations for typically 50 000 (about 7 ps) steps to calculate the Born terms, and 150 000–200 000 (about 22 to 30 ps) steps to calculate the stress fluctuation terms. Results of such calculations in the temperature range of 300 K to 2000 K are shown in Fig. 10. For comparison, we also show the elastic constants obtained from the original Tersoff potential and available measurements. No direct experimental data of elastic constants of single crystal β-SiC at elevated temperatures are available. The solid lines in the figure are fitted functions using data obtained from polycrystalline β-SiC samples.[34] On the other hand, the experimental elastic constants for single crystal β-SiC at room temperature are available[35] and are shown as stars in the figure. As the comparison shows, significant improvement of the elastic constants at elevated temperatures is achieved by the modified Tersoff potential. For the temperature range under study, all elastic constants show the expected thermal softening behavior;[36] and they can be well fitted as linear functions of temperature. Results of the linear coefficients obtained from fitting are summarized in Table V, which shows that the modified Tersoff potential predicts satisfactory elastic constants behavior at elevated temperatures. Combining this result with the equation of state (Fig. 7), we conclude that the modified potential provides a reasonably good description of mechanical properties of β-SiC at finite stress and elevated temperatures.

As shown in the 0 K elastic constants calculations, a significant contribution to the shear elastic constant C_{44} comes

TABLE V. Variation coefficients of elastic constants as a function of temperature (in units of GPa/°C).

	dC_{11}/dT	dC_{12}/dT	dC_{44}/dT
Present study	-0.036	-0.0046	-0.038
Li and Bradt (Ref. 30)	-0.025	-0.011	-0.007

from the internal strain relaxation. Using the fluctuation formulas, the internal strain relaxation is calculated by the stress fluctuation term.[18] In Fig. 11, we show contributions to the total elastic constants from individual terms, i.e., the Born term and the stress fluctuation term. We ignore the constant kinetic terms here since they are orders of magnitude smaller. One can see that the stress fluctuation contribution in C_{44} is much larger than those in C_{11} and C_{12}. This demonstrates that internal strain relaxation is taken into account by the stress fluctuation term through MD simulations.

E. Surface relaxation and reconstruction

Besides considering only bulk properties, we can test the transferability of the Tersoff potential by analyzing surface properties of β-SiC. We have calculated surface energies and studied (100), (110), and (111) surface relaxation at low temperatures. For surface reconstruction, only the (100) surface was treated owing to its simplicity and the availability of experimental and tight-binding results. For (100) and (111) surfaces, both C-terminated and Si-terminated surfaces are investigated.

To set up the initial geometry for surface studies, the minimum number of repeatable stacking layers along each direction in the zinc-blende structure is used as a layer unit. The number of layers in each layer unit is 4, 2, and 6, respectively, along the (100), (110), and (111) directions, and we use 2, 2, and 3 layer units for the studies of (100), (111), and (110) surfaces, respectively. Along the (100) and (110) directions, layers are uniformly spaced; along the (111) direction, layers are alternately spaced at two distances of l and $l/3$, where l is the bond length between Si-C. A plane that cuts through the shorter spacing is called a *glide plane*, while a plane that cuts through the longer spacing is called a *shuffle plane*. Within each layer, approximately 10–20 atoms are used. Periodic boundary conditions are applied only along the two directions (y and z) that are parallel to the surfaces. Along the direction (x) perpendicular to the surface, atoms

TABLE VI. Comparison of bond-order parameter b_{ij} as a function of local coordination number for i=C (first row) and i=Si (second row).

	Bulk	Shuffle (111) [or (110)]	(100)	Glide (111)
Coord. no.	4	3	2	1
C	0.8663	0.8917	0.9234	0.9776
Si	0.9368	0.9475	0.9599	0.9776

in the bottom layer unit are fixed in order to model a bulk material with one free surface at the top. The structures thus constructed are found to be thick enough since the results show that almost all the surface relaxation and reconstruction involve only atoms in the top two layers. All relaxation and reconstruction studies are performed by molecular dynamics simulations at 10 K.

The surface energy is defined as $\gamma_e=(E_s-E_b)/A$, where E_s and E_b denote potential energy per atom in the bulk and at the surface, respectively; A is the exposed surface area per atom. Physically, γ_e is the energy increase due to dangling bonds. For an unrelaxed surface, γ_e is simply determined by the negative binding energy of the dangling bonds for pair potentials. However, for the many-body Tersoff potential, the situation is different. As atoms lose bonds at the surface, the remaining bonds automatically strengthen themselves even without relaxation of atomic positions. This is due to the many-body nature of the potential, where the strength of each bond is determined by the local atomic configuration and the bond-order parameter b_{ij} is a function of local coordination number. A summary of b_{ij} at different surfaces is shown in Table VI, where one clearly sees that the remaining bonds strengthen themselves as b_{ij} increases when the coordination number decreases at different surfaces. The results of unrelaxed surface energies of β-SiC are given in Table VII. The shuffle-(111) surface has the lowest surface energy. This is to be expected since the shuffle-(111) surface has the lowest density of bonds. The only experimental value of surface energy reported in the literature to our knowledge is 2180 erg/cm^2 by Oshcherin,[37] which agrees with our result of 2525 erg/cm^2 very well.

Since atoms at the surfaces that are ideally truncated are undercoordinated, they will experience nonzero net forces and will relax to new equilibrium positions. This is the process of surface relaxation. We find that relaxation of (100) and (111) surfaces only involves vertical displacements of atoms, whereas both vertical and lateral displacements are involved for (110) surface. In Table VIII, results of energy decrease and vertical displacement of atoms during surface relaxation are summarized. Also shown in the table are results obtained using the Pearson potential, tight-binding calculation,[38] and *ab initio* calculation.[39] The vertical displacements given in this table are averaged over all atoms in the layer. For the energy decrease dE, the Tersoff potential gives better results for Si (100), Si (111), and (110) surfaces, while the Pearson potential gives better results for C (100) and C (111). We believe that this is because the latter has incorporated some C cluster information in the fitting procedures. For the displacements of dH_1, dD_{12} and dH_2, the Tersoff potential consistently gives better results than the Pearson potential. Also, dH_1 and dD_{12} from the Tersoff potential are in excellent agreement with the tight-binding calculations. For the (100) and (111) surface relaxation, the C surfaces exhibit larger inward displacements and gain more energy than the Si surfaces. For all surfaces, contraction of the top two layers during relaxation is observed.

TABLE VII. Unrelaxed surface energies of β-SiC calculated using the modified Tersoff potential.

Planes	Energy (erg/cm^2)
shuffle (111)	2525
(110)	3093
(100)	4618
glide (111)	8219

TABLE VIII. Summary of energy decrease and vertical layer displacements due to surface relaxation of β-SiC. dE is the energy decrease per atom; dH_n is the averaged atomic displacement from its bulk position in the nth layer; and dD_{mn} is the change in percentage of interlayer spacing between nth and mth layers compared to their bulk spacing. Negative (or positive) sign represents inward (or outward) movement toward (or away from) the bulk.

	TP	PP	TB	*ab initio*
C (100) relaxation				
dE (ev/atom)	0.49	0.25	0.34	
dH_1 (Å)	−0.17	−0.15	−0.17	
dD_{12} (%)	−23.0	−14.0	−22.0	
dH_2 (Å)	0.04	−0.01	0.07	
Si (100) relaxation				
dE (eV)	0.09	0.18	0.02	
dH_1 (Å)	−0.04	−0.07	−0.04	
dD_{12} (%)	−6.2	−8.4	−4.6	
dH_2 (Å)	0.03	−0.02	0.01	
C (111) relaxation				
dE (eV)	0.83	0.62	0.43	
dH_1 (Å)	−0.27	−0.30	−0.21	
dD_{12} (%)	−51.2	−61.2	−52.4	
dH_2 (Å)	0.05	0.08	0.12	
Si (111) relaxation				
dE (eV)	0.11	0.31	0.03	
dH_1 (Å)	−0.04	−0.06	−0.05	
dD_{12} (%)	−11.8	−20.5	−11.1	
dH_2 (Å)	0.03	0.06	0.02	
(110) relaxation				
dE (eV)	0.29	0.41		0.21
dH_1 (Å)	−0.17	−0.15	−0.17	
dD_{12} (%)	−23.0	−14.0	−22.0	
dH_2 (Å)	0.04	−0.01	0.07	

For the (110) surface, there are both Si and C atoms in the top layer and they move differently in the relaxation process. Though the averaged displacement shows inward relaxation, the actual displacements of Si and C atoms are different. Relaxation of the (110) surface is more complicated than that of (100) and (111) surfaces because it involves atomic dis-

TABLE IX. Relaxation and buckling of the (110) surface of β-SiC. dX is the vertical displacement of the top layer atoms and dY and dZ are the lateral displacements of the top layer atoms. dE is the average energy gain per atom.

	TP		PP		TB		*ab initio*	
dE (eV)	0.29		0.41				0.21	
	C	Si	C	Si	C	Si	C	Si
dX (Å)	−0.22	0.03	−0.27	−0.01	−0.12	−0.21	−0.05	−0.17
dY (Å)	0.00	0.00	0.00	0.00			0.00	0.00
dZ (Å)	−0.18	0.01	0.21	0.02			0.02	−0.14

placements in the lateral directions. In Table IX, the results of relaxation of the (110) surface are summarized and compared with the tight-binding calculation[38] and *ab initio* calculation.[39] The calculated energy gain from the Tersoff potential is in close agreement with the *ab initio* calculation. However, the Tersoff potential predicts inward relaxation of C atoms, and slight outward relaxation of Si atoms, which are different from the predictions of tight-binding and *ab initio* calculations. The latter two methods predict inward relaxation of both C and Si atoms with larger displacement for Si atoms. This relaxation process requires proper treatment of electron transfer and charge effects[39,38] which are absent in the Tersoff potential. Thus its failure to predict the correct buckling behavior of the (110) surface is understandable. Note that, though the Pearson potential predicts inward relaxation for both C and Si atoms, the relative amount of displacement is not correct compared with the tight-binding and *ab initio* results.

Another important aspect of surface relaxation involves a symmetry change in the surface layer relative to the bulk structure. This is the process of *surface reconstruction*. Surface reconstruction of (100) surfaces of β-SiC has been studied by scanning tunneling microscopy (STM)[40] and low-energy electron diffraction[41] (LEED) experiments. Several reconstruction patterns have been observed. Two typical ones are the 2×1 and 2×2 reconstructions. We have studied the (100) surface of β-SiC using the Tersoff potential and the Pearson potential. We first intentionally move the atoms towards the expected reconstruction sites to help the system to overcome the energy barrier and also make simulations more efficient at low temperature. Then we allow atoms to relax to new equilibrium positions by MD simulations. If no reconstruction is energetically favored, we find atoms move back to their initial equilibrium positions. In this way we have observed 2×1 and 2×2 dimer formation on both C (100) and Si (100) surfaces using the Tersoff potential. For the Pearson potential, no 2×1 dimers are observed on the Si (100) surface. In Table X, we summarize the results from the Tersoff potential, the Pearson potential, and the tight-binding calculation.[38] From the bond lengths and energy gain, we find that the 2×1 reconstruction is favored over the 2×2 reconstruction, which is in agreement with the tight-binding calculation. However, from the tight-binding calculations, the bond length of Si dimers (2.16 Å) is smaller than the bond length in diamond cubic Si (2.35 Å), and the bond length of C dimers (1.74 Å) is larger than that in diamond C (1.54 Å). For the Tersoff potential, the opposite situation is obtained. Though the Tersoff potential is able to predict the low energy 2×1 reconstruction successfully, the quantitative results are not satisfactory. It appears that surface reconstruction involves significant electronic structure effects, which cannot be described properly by any empirical potentials.

IV. DISCUSSIONS

Based on the various bulk and surface properties of β-SiC presented in this paper, we demonstrate that the bond-order potential developed by Tersoff is able to describe the angle-dependent forces reasonably well, provided that only the nearest-neighbor interactions between Si and C are taken into account. The modified Tersoff potential gives satisfactory results for the acoustic phonon dispersion curves, equation of state, thermal expansion coefficient, and elastic constants variations with temperature. In our opinion, the reasons for the success of this potential can be attributed to its ability to describe well the volumetric variation of the cohesive energy (as can be seen in Fig. 3) and to its bond-order nature. It is also noteworthy to recall that the only specific property of the compound (as opposed to properties of the elemental constituents Si and C) which enters into the potential is the heat of formation, and it is used to determine the strength of the heteropolar bond relative to a simple interpolation. Moreover, the Tersoff potential predicts correct surface energy for β-SiC, where the shuffle-(111) surface has the lowest surface energy. It also predicts fair energy gain

TABLE X. Surface reconstruction of the (100) surfaces of β-SiC. r is the bond length (in units of Å); dE is the energy gain (in units of eV); and dL is the top layer lateral displacement (in units of Å).

	dE		r		dL	
	2×1	2×2	2×1	2×2	2×1	2×2
C (100)						
TP(SiC)	2.42	2.29	1.48	1.49	±0.79	±0.78
PP(SiC)	2.97	2.90	1.49	1.49	±0.74	±0.73
TB(SiC)	2.31		1.74		±0.67	
Si (100)						
TP(SiC)	0.67	0.63	2.46	2.54	±0.30	±0.26
PP(SiC)	No Dimer	0.41	No Dimer	2.49	No Dimer	±0.24
TB(SiC)	1.03		2.16		±0.45	

and excellent vertical displacements for (100) and (111) surface relaxation. However, due to the absence of proper treatment of electron transfer and the resulting charge effect, the Tersoff potential cannot account for the correct buckling behavior of the (110) surface relaxation and the splitting of the optic phonon modes at the Γ point. Currently, none of the empirical potentials for SiC deal with the charge effect explicitly, though the inclusion of Coulomb interaction into the two-body potential part is possible.[23]

Although the current modification of the Tersoff potential is successful to some extent, we believe that it is desirable to take into consideration the Si-Si and C-C interactions in the fitting procedure for β-SiC. As we have discovered, the unphysical effect is the large repulsion between the Si-C bond due to second-nearest-neighbor interactions at small angles. Proper fitting of the angular function for the β-SiC structure could resolve this problem. Incorporating the Si-Si and C-C interactions in β-SiC in the fitting should give a better description of the disordered structures of SiC, such as molten and amorphous SiC. In the original Tersoff potential, these states were not considered. In our modification, fitting the melting temperature of β-SiC implicitly brings in some effects of the Si-Si and C-C interactions. Also, our scheme of introducing the variable cutoff can be extended by considering local cutoffs scaling with local instead of global volume. The variable cutoffs may be useful for heterogeneous deformation.

ACKNOWLEDGMENTS

This work has been supported by AFOSR Grant No. 91-0285. One of us (M.T.) acknowledges support from MIT. We are grateful to E. Kaxiras for providing us with the total energy results obtained by first-principles calculation. We also acknowledge early contributions to develop the molecular dynamics simulation code for Tersoff potential by E. Burke. Computations were carried out in part under allocations from the San Diego Supercomputer Center.

[1] T. Nguyen, P. S. Ho, T. Kwok, C. Nitta, and S. Yip, Phys. Rev. B **46**, 6050 (1992).
[2] K. S. Cheung and S. Yip, Modeling Simul. Mater. Sci. Eng. **2**, 865 (1994).
[3] V. Bulatov, S. Yip, and A. Argon, Philos. Mag. A **72**, 496 (1995).
[4] H. Balamane, T. Halicioglu, and W. A. Tiller, Phys. Rev. B **46**, 2250 (1992).
[5] F. Finocchi, G. Galli, M. Parrinello, and C. M. Bertoni, Phys. Rev. Lett. **68**, 3044 (1992).
[6] P. C. Kelires, Europhys. Lett. **14**, 43 (1991).
[7] M. Kohyama, S. Kose, M. Kinoshita, and R. Yamamoto, J. Phys. Condens. Matter **2**, 7791 (1990).
[8] M. Tang and S. Yip, J. Appl. Phys. **76**, 2719 (1994).
[9] M. Tang and S. Yip, Phys. Rev. Lett. **75**, 2738 (1995).
[10] M. Tang, Ph.D. thesis, Massachusetts Institute of Technology, 1995.
[11] A. El-Azab and N. M. Ghoniem, Radiat. Effects Defects Solids **129**, 117 (1994).
[12] J. Tersoff, Phys. Rev. B **39**, 5566 (1989).
[13] E. Pearson, T. Takai, T. Halicioglu, and W. A. Tiller, J. Cryst. Growth **70**, 33 (1984).
[14] M. I. Baskes (unpublished).
[15] J. Tersoff, Phys. Rev. B **27**, 6991 (1988); **38**, 9902 (1988).
[16] J. Tersoff, Phys. Rev. Lett. **61**, 2879 (1988).
[17] M. Parrinello and A. Rahman, J. Appl. Phys. **52**, 7182 (1981).
[18] J. R. Ray, Comput. Phys. Rep. **8**, 109 (1988).
[19] G. C. Abell, Phys. Rev. B **31**, 6184 (1985).
[20] A. Isik, Ph.D. thesis, Massachusetts Institute of Technology, 1994.
[21] J. H. Rose, J. R. Smith, F. Guinea, and J. Ferrante, Phys. Rev. B **29**, 2963 (1984).
[22] E. Kaxiras (private communication).
[23] D. H. Lee and J. D. Joannopoulos, Phys. Rev. Lett. **48**, 1846 (1982).
[24] H. M. J. Smith, Proc. R. Soc. London Ser. A **241**, 105 (1948).
[25] D. W. Feldman, J. H. Parker, W. J. Choyke, and L. Patrick, *ibid.* **173**, 787 (1968); **170**, 698 (1968); W. J. Choyke, D. R. Hamilton, and L. Patrick, Phys. Rev. **133**, A1163 (1964).
[26] E. O. Kane, Phys. Rev. B **31**, 7865 (1985).
[27] W. A. Bassett, M. S. Weathers, and T. C. Wu, J. Appl. Phys. **74**, 3824 (1993).
[28] M. Yoshida, A. Onodera, M. Ueno, K. Takemura, and O. Shimomura, Phys. Rev. B **48**, 10 587 (1993).
[29] F. Birch, J. Geophys. Res. **83**, 1257 (1978).
[30] Z. Li and R. C. Bradt, J. Mater. Sci. **21**, 4366 (1986).
[31] M. Born and K. Huang, *Dynamical Theory of Crystal Lattice* (Clarendon, Oxford, 1956).
[32] K. Mizushima, S. Yip, and E. Kaxiras, Phys. Rev. B **50**, 14 952 (1994).
[33] C. S. G. Cousins, J. Phys. C **11**, 4867 (1978); **11**, 4881 (1978).
[34] Z. Li and R. C. Bradt, J. Mater. Sci. **22**, 2557 (1987).
[35] W. R. L. Lambrecht, B. Segall, M. Methfessel, and M. van Schilfgaarde, Phys. Rev. B **44**, 3685 (1991).
[36] K. S. Cheung, A. Argon, and S. Yip, J. Appl. Phys. **69**, 2088 (1991); J. H. Wang, Ph.D. thesis, Massachusetts Institute of Technology, 1993.
[37] B. N. Oshcherin, Phys. Status Solidi A **34**, K181 (1976).
[38] S. P. Mehandru and A. B. Anderson, Phys. Rev. B **42**, 9040 (1990).
[39] D. H. Lee and J. D. Joannopoulos, J. Vac. Sci. Technol. **21**, 351 (1982).
[40] C. S. Chang, N. J. Zheng, S. T. Tsong, Y. C. Wang, and R. F. Davis, J. Vac. Sci. Technol. B **9**, 681 (1991).
[41] R. Kaplan, Surf. Sci. **215**, 111 (1989).